Available online at www.sciencedirect.com
ScienceDirect
Remote Sensing of Environment 107 (2007) 185–193
Remote Sensing of Environment
www.elsevier.com/locate/rse

Cloud model evaluation using radiometric measurements from the airborne multiangle imaging spectroradiometer (AirMISR)

Mikhail Ovtchinnikov *, Roger T. Marchand

Pacific Northwest National Laboratory, Richland, WA, United States

Received 1 March 2006; received in revised form 25 May 2006; accepted 31 May 2006

Abstract

Detailed information on cloud properties is needed to rigorously test retrieval algorithms for satellite and ground-based remote sensors. The inherent complexity of clouds makes this information difficult to obtain from observations alone and cloud resolving models (CRMs) are often used to generate synthetic datasets that can be used as proxies for real data. We test the ability of a CRM to reproduce the observed structure of low-level clouds detected by the Earth Observing System (EOS) validation program in north central Oklahoma on March 3, 2000. A three-dimensional radiative transfer model is applied to high-resolution cloud fields generated by the CRM in order to simulate the top of atmosphere radiances. These synthetic radiances are then statistically compared with observations from the airborne Multiangle Imaging SpectroRadiometer (AirMISR), flown on the NASA ER-2 high-altitude aircraft. Simulations match well the blue channel radiance distributions at oblique view angles but overestimate the minimum in reflectance at near-nadir viewing angles. The model reproduces correctly the angular change in the width of radiance distribution, as measured by the standard deviation but the change in skewness of these distributions is captured only qualitatively. The model biases are suggestive of the simulated cloud boundaries being too sharp and the distribution of the vertical liquid water path being too narrow. A power spectrum analysis shows a close agreement between simulations and observations including a break in the scaling properties of the radiance fields around 400 m. The scaling properties of the 1D power spectrum of simulated radiance at smaller scales exhibit directional dependence not seen in corresponding observations.

Keywords: 3D radiative transfer; AirMISR; Retrieval algorithms

1. Introduction

Detailed information on cloud structure and cloud properties is needed to rigorously test retrieval algorithms for satellite and ground-based remote sensors. Unfortunately, the inherent complexity of clouds makes this information difficult to obtain from observations alone. Cloud resolving models (CRMs) are becoming a tool of choice for generating synthetic cloud fields that can be used as proxies for real data. By providing detailed and physically consistent description of the atmospheric state, CRM simulations are now extensively used to develop and test retrieval algorithms using radiometric measurements from satellite (e.g., Kato et al., 2006) and ground-based systems (e.g., Barker et al., 2004). In order to increase the reliability of this approach, the ability of CRMs to reproduce the observed structure and radiometric characteristics of clouds at wide range of scales has to be quantified.

Many studies have compared model-generated cloudiness with satellite observations, focusing primarily on analysis of retrieved and highly integrated cloud characteristics. Such studies yield useful results when applied to synoptic systems in global and mesoscale modeling. Indeed, cyclones, hurricanes, atmospheric fronts, and even individual thunderstorms can be easily and unmistakably identified from satellite imagery. The situation, however, changes drastically when the focus shifts to internal structure of clouds and smaller scales. Even a seemingly simple determination whether a pixel should be categorized as “clear” or “cloudy” is subjective in a sense that this is typically done by comparing measured radiance to some preset threshold value. This inherent ambiguity of the derived satellite products can be avoided by using the raw radiances, i.e. the measurements, rather than derived products, such as cloud fraction, retrieved optical depth, or effective droplet radius.

* Corresponding author. Pacific Northwest National Laboratory, PO Box 999, Richland, WA 99352. Tel.: +1 509 375 2514; fax: +1 509 375 6448.
E-mail address: mikhail@pnl.gov (M. Ovtchinnikov).

0034-4257/$ - see front matter © 2007 Elsevier Inc. All rights reserved.
doi:10.1016/j.rse.2006.05.024

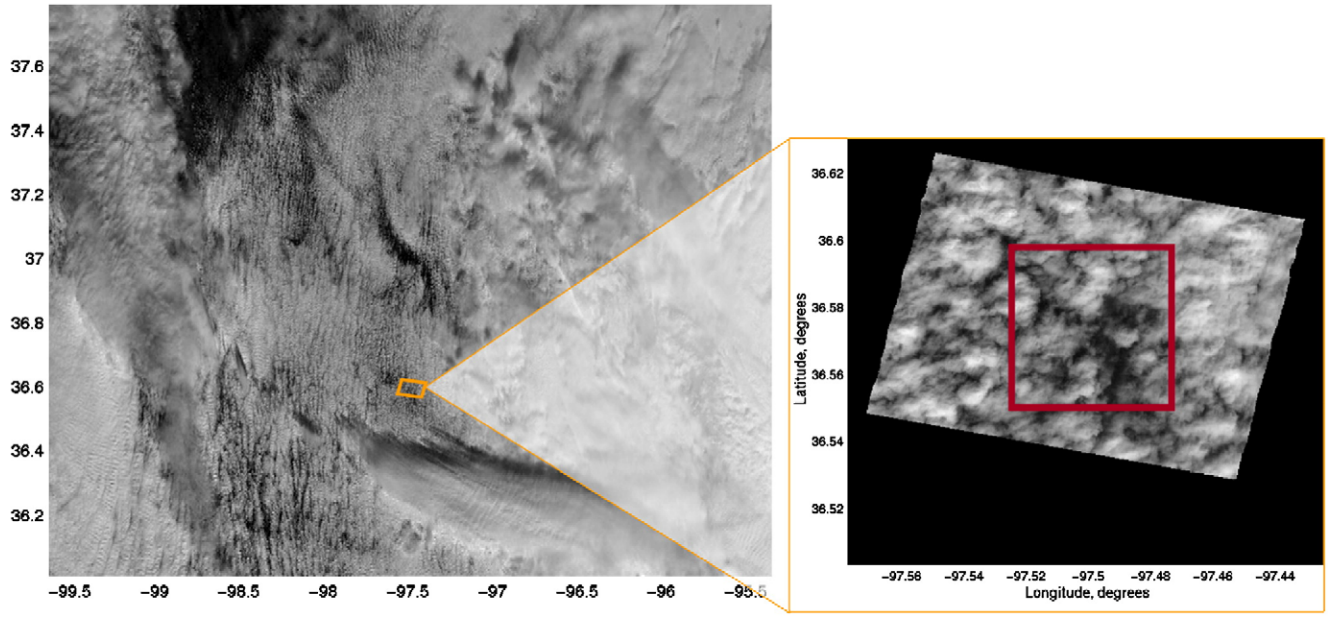

Fig. 1. The cloud scene over the ARM Central Facility at 17:39 UTC March 3, 2000 as viewed by the nadir pointing cameras from MISR (left panel) and AirMISR right panel. Red square on the right panel illustrates horizontal size of the model domain (5 km × 5 km). (For interpretation of the references to colour in this figure legend, the reader is referred to the web version of this article.)

To date, raw radiances have rarely been used in model validation studies and, to our knowledge, only with respect to global and mesoscale models (e.g., Chevallier & Kelly, 2002; Morcrette, 1991). Yet, recent advances in cloud and radiative transfer modeling combined with increasing computer power make it possible to compute solar reflectance for cloudy atmosphere at high horizontal resolution. Barker et al. (2003) simulated nadir reflectances for a CRM-generated boundary layer cloud deck but the realistically looking fields were not compared to observations. Zuidema et al. (2003) and Marchand and Ackerman (2004) performed closure studies in which simulated angular dependences of reflectance were compared to Multiangle Imaging SpectroRadiometer (MISR) observations of cumulus congestus and stratocumulus, respectively. The three-dimensional distributions of clouds in these cases, however, were reconstructed from observations, including those from MISR, rather than simulated by a CRM.

In this study, we use multiangular radiance distributions measured by the airborne version of MISR (AirMISR) to evaluate the structure of continental stratocumulus simulated by a high-resolution cloud resolving model. While the CRM cannot be expected to reproduce any particular cloud scene exactly, the observed and simulated cloud fields should have the same statistical properties. By comparing the statistics of the simulated radiance fields with the statistics of the actual AirMISR measurements we aim to establish the fidelity of the high-resolution cloud model.

2. Dataset and model descriptions

2.1. Observational datasets

On March 3, 2000, low and middle level clouds formed over the Atmospheric Radiation Measurement program (ARM) Southern Great Plains (SGP) site in the wake of a cold front. As part of the NASA's Earth Observing System (EOS) validation campaign and ARM cloud intensive operational period (IOP), ground remote sensing observations and aircraft measurements (both in and above clouds) were coordinated with Terra overpass. By 17:39 UTC, the time of Terra satellite overpass, the middle-level clouds had drifted away and the ARM site was covered by single-layer low clouds (Fig. 1, left panel). The NASA high altitude ER-2 aircraft carrying AirMISR on board followed Terra's ground track and over flew the ARM central facility site (36.607 N, 97.488 W) at 17:39:10 UTC. It takes about 9 min for AirMISR to image any location from all nine MISR-like view angles. Unlike MISR, which has a separate camera for each viewing angle (Diner et al., 2002, 2005), AirMISR uses a single turning camera (Marchand et al., 2001). Therefore, only one scene is sampled by AirMISR over the 17:33–17:45 UTC flight segment providing the angular distribution of radiances for only a relatively small

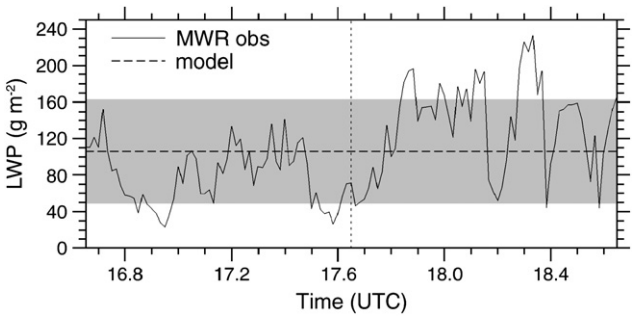

Fig. 2. One-minute averaged liquid water path (LWP) derived from the microwave radiometer (MWR) at the ARM central facility over 2 h around the time of the AirMISR overpass indicated by the vertical dotted line. Shaded area indicates the domain average of the model LWP field used in the calculations (horizontal dashed line) plus and minus one standard deviation.

Table 1
Zenith and scattering angles for the nine AirMISR cameras

Camera	DF	CF	BF	AF	AN	AA	BA	CA	DA
Direction	Fore				Nadir	Aft			
Zenith angle, ξ (°)	70.5	60.0	45.6	26.1	0.0	26.1	45.6	60.0	70.5
Scattering angle (°)	72.3	81.8	94.9	112.5	135.0	152.5	154.6	148.1	140.8

Scattering angle is the angle between directions of photons traveling from the sun and toward the camera. Scattering angles are calculated for the solar zenith angle of 45° and the sun-sensor azimuth difference of 36 and 144° for the fore and aft cameras, respectively.

region around the ARM central facility (on the order of 10×10 km^2; Fig. 1 right panel). The benefit of using these data is in the much higher resolution (27.5 m) of the AirMISR imagery compared to the MISR imagery (275 m), which is, of course, a direct consequence of the lower flying altitude of ER-2 (20 km) compared to that of Terra (705 km).

2.2. Cloud resolving simulation

The cloud resolving model used in this study is that of Khairoutdinov and Randall (2003). The model is run in a large-eddy simulation (LES) mode with a bulk treatment of the cloud microphysics. The model domain consists of $200\times200\times160$ grid cells covering $5\times5\times3.2$ km^3 physical domain with uniform 25-m horizontal and 20-m vertical resolutions. Periodic boundary conditions are used in both horizontal directions. In order to account for changes in the environment due to synoptic-scale circulation, which are important for simulations over several hours, prescribed tendencies are imposed on temperature and moisture fields and horizontal wind components are nudged toward observations. Latent and sensible surface heat fluxes are prescribed based on observations at the ARM SGP site. The forcing is the same as used in a recent model intercomparison study, which focused on simulating the frontal passage over the ARM SGP site on 2–3 March 2000 (Xie et al., 2005). The simulation setup is different in that we run the model at much higher resolution on a smaller domain and for a shorter period of time, concentrating on the fine-scale structure of post-frontal low-level clouds. Our CRM simulation begins at 15:00 UTC on March 3, 2000 and lasts for 4 h. A snapshot of the cloud field at 18:00 UTC serves as input to 3D radiation calculations described below. At that time, the vertical liquid water path (LWP) has the domain mean value of 106 g m^{-2} and standard deviation of 57 g m^{-2}. This compares favorably with the LWP retrieved from the microwave

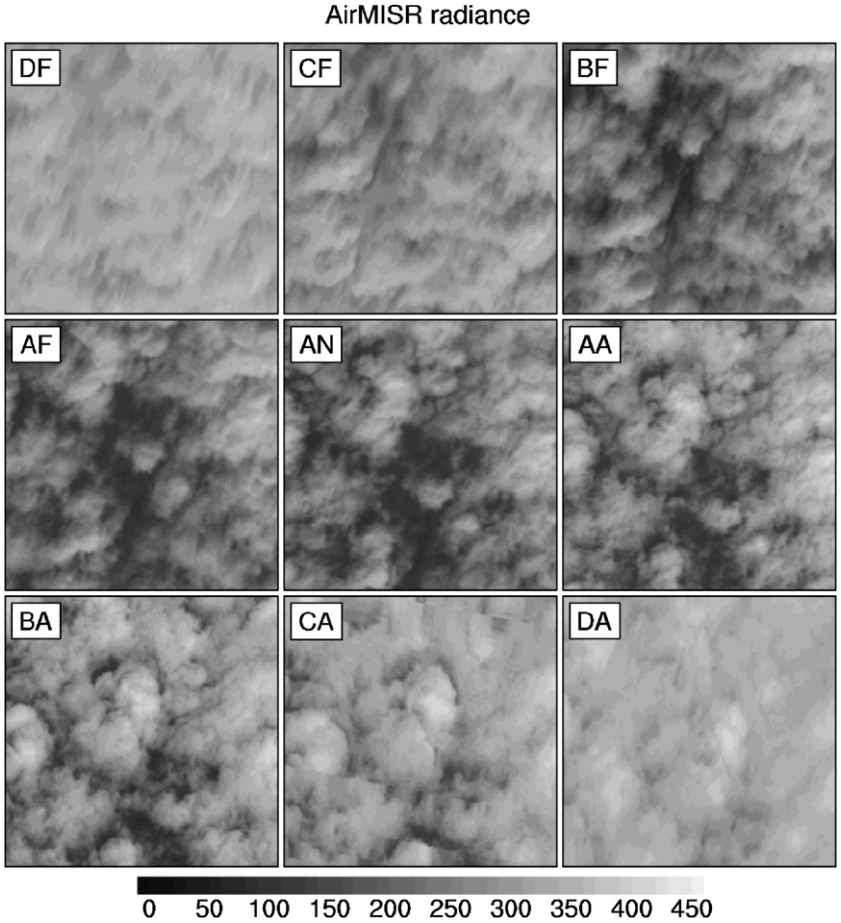

Fig. 3. Observed blue channel ($\lambda=0.443$ μm) radiances (W m^{-2} μm^{-1} sr^{-1}) for the nine AirMISR cameras listed in Table 1. Each panel consists of 200×200 pixels at 27.5 m resolution.

radiometer (MWR) located at the ARM Central Facility (Fig. 2). The retrieved LWP has a 2-hour mean of 107 g m^{-2} with the standard deviation for one-minute samples of 50 g m^{-2}.

2.3. 3D radiative transfer

Simulated radiances are obtained using the Spherical Harmonic Discrete Ordinate Method (SHDOM) radiation transfer code (Evans, 1998). SHDOM is run in full 3D mode with cyclic boundary conditions using $N_{\text{zenith}}=16\times N_{\text{azimuth}}=32$ discreet ordinates. Monochromatic radiances are computed for 0.443 μm wavelength (the "blue" AirMISR channel) for which molecular Rayleigh scattering is accounted for and gaseous absorption is neglected. The surface is treated as Lambertian with albedo of 0.04, based on spectral albedo measurements around the SGP site in March 2000. Spatial distribution of the cloud water is taken from the CRM. In computations of the extinction cross section, single scattering albedo, and phase function using Mie theory the droplet size spectrum is assumed to follow a gamma distribution with effective variance of 0.1 (a shape parameter of 7) and effective radius of 6.8 μm. The latter is derived from averaging in-cloud measurements using the forward scattering spectrometer probe (FSSP) on board of the University of North Dakota Citation aircraft. The resulting optical depth of the simulated cloud field of 23 agrees with the independently derived estimate from GOES 8 retrieval of 19.7±3.9. The computational domain includes all layers containing liquid water plus two layers below the cloud base and five layers between the highest cloud top and 20 km. The geometry of the radiation simulation matches the AirMISR–Sun configuration. The solar zenith angle is set to 45° and the solar azimuth is 105°. The plane track is 36° off the solar principle plane. Zenith and scattering angles corresponding to the nine AirMISR cameras are given in Table 1. In computing radiances for the nine camera angles we neglect the evolution of the cloud field and the change in Sun's position during the 9 min it takes for the AirMISR to sample the study area.

3. Results

Figs. 3 and 4 show the observed and simulated blue channel radiances for all nine viewing angles. There are obvious similarities between the two sets of images. The near-nadir views (AF, AN, and AA camera angles) show cloud elements of similar horizontal size with dark ground seen in-between. Cloud gaps become progressively less visible as viewing angle increases and close nearly completely at the most oblique views (DF and DA cameras).

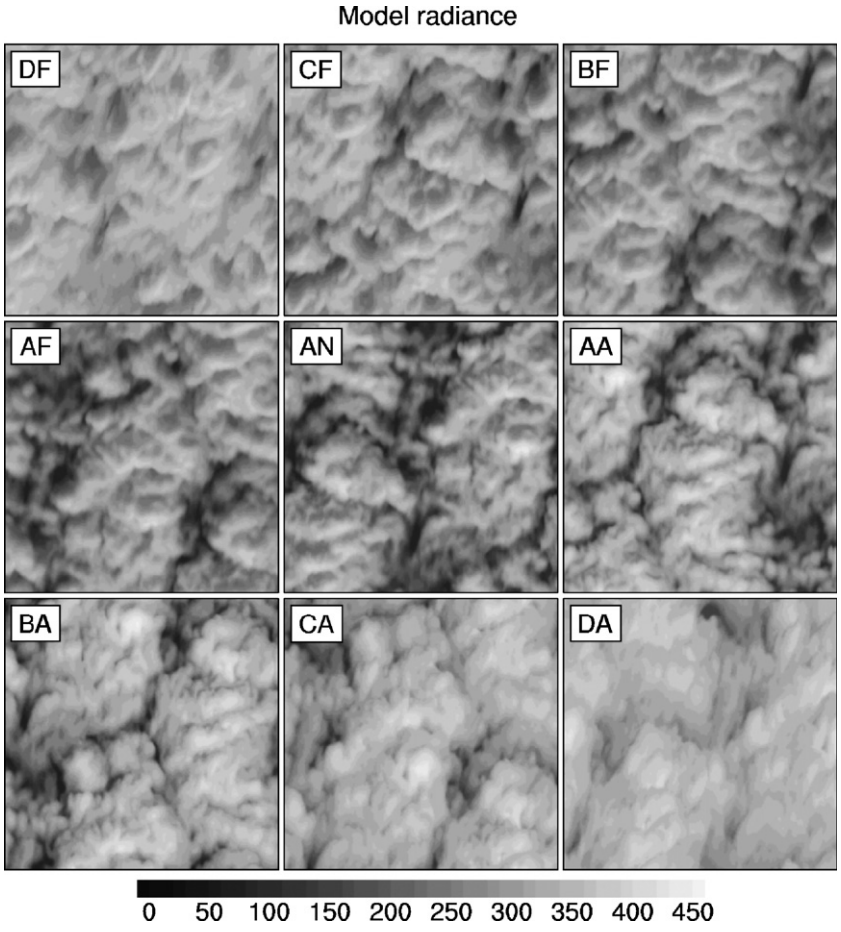

Fig. 4. Simulated blue channel ($\lambda=0.443$ μm) radiances (W m^{-2} μm^{-1} sr^{-1}) for the nine AirMISR cameras listed in Table 1. Each panel consists of 200×200 pixels at 25 m resolution.

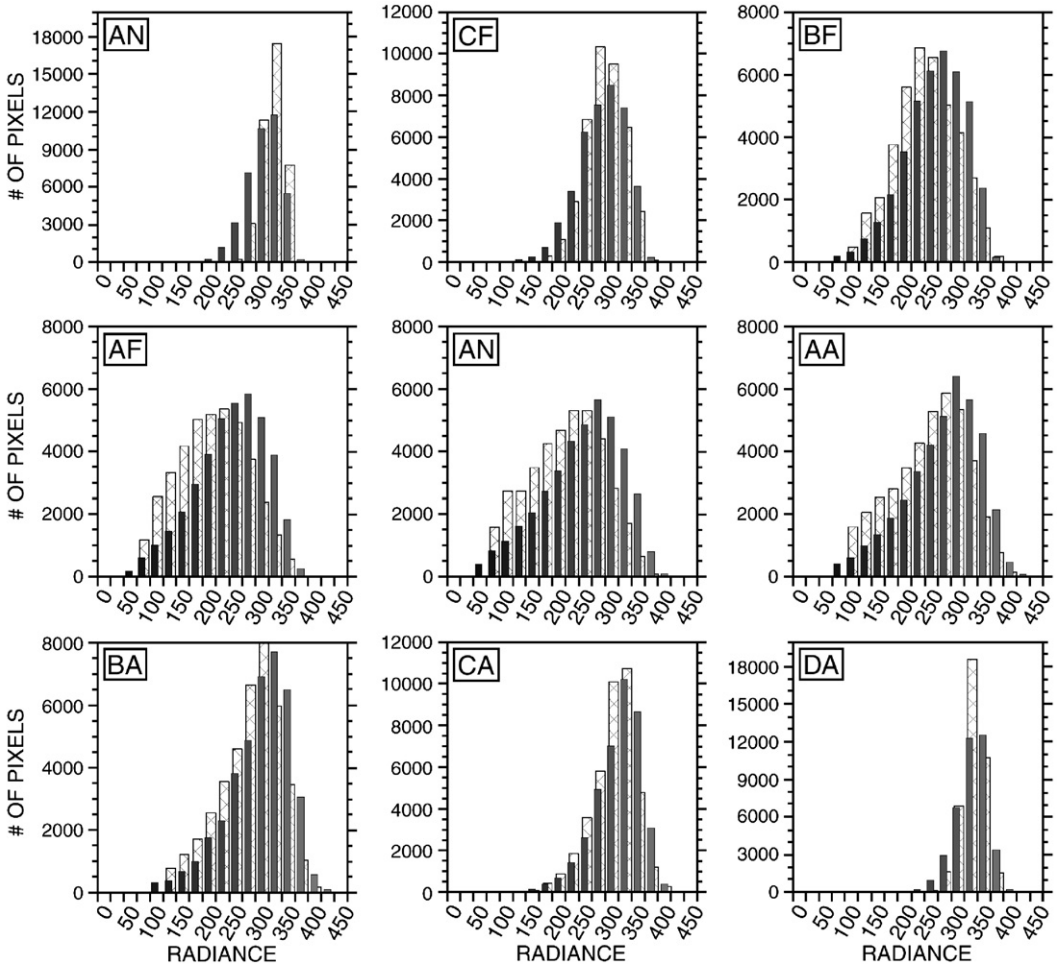

Fig. 5. Histograms of the observed (hatched) and simulated (filled) radiances (W m^{-2} μm^{-1} sr^{-1}) at nine AirMISR viewing angles.

A closer look also reveals notable differences between the model and observations. On the larger scale, clouds on the AirMISR images lack an obvious preferential orientation but the simulated images show well defined rolls aligned with the wind along the north–south direction. This discrepancy is not indicative of any model shortcoming, however. In fact, the model appears to respond correctly to large-scale forcing by developing the rolls, which were observed just to the west and to the north of the SGP CF (Fig. 1, left panel). The size of the model domain and its periodicity in horizontal directions can affect the width and alignment of the rolls but in this case of predominantly northerly wind the orientation of these patterns is captured correctly.

Another difference on the smaller scale is that the transition from cloud to clear air at nadir view appears to be sharp in the simulation and more subtle in observations. Larger fraction of pixels with small near-nadir radiances in the AirMISR images compared to the simulations is illustrated by the respective histograms (panels AF, AN, and AA in Fig. 5). The observed radiance distributions for these angles are more symmetrical than the modeled ones, which are skewed toward the larger values. The mean simulated radiances for small zenith view angles are overestimated. At off nadir angles, the model captures well both the shape and position of much narrower distributions.

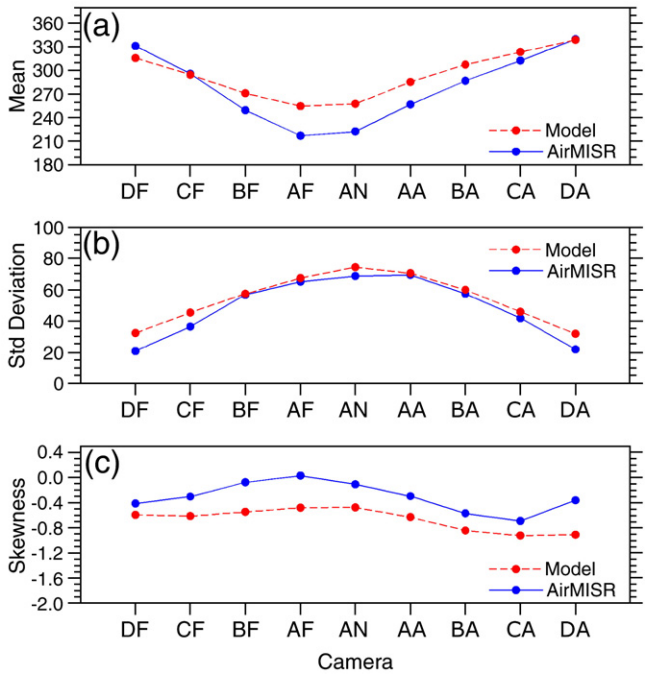

Fig. 6. Means (W m^{-2} μm^{-1} sr^{-1}), standard deviations (W m^{-2} μm^{-1} sr^{-1}), and skewnesses for the observed and simulated radiance distributions from Figs. 3 and 4, respectively.

Fig. 6a illustrates more clearly the angular dependence of the mean radiance. It quantifies the visual observation from Figs. 3 and 4 that the simulated clouds are brighter than the real ones at near-nadir angles. The model and observations both show a minimum in the mean radiance at the AF and AN view angles, but the model overestimate the reflectance at these view angles. The increased reflectance at larger viewing angles compared to nadir (AN camera) is driven primarily by the cloud optical path, which for plane parallel clouds is proportional to $1/\cos(\xi)$ where ξ is the zenith viewing angle. The asymmetry in the angular distribution of the mean radiance about the AN view is the result of a minimum in the phase function, which for small droplets is located near 105° or between scattering angles corresponding to BF and AF directions (Table 1).

The variability of the fields represented by the standard deviation of radiance distributions decreases from its maximum at nadir view angle toward much smaller values at larger view angles (Fig. 6b), at which breaks in the cloud fields are closed by the cloud sides. The model distributions have slightly larger standard deviations and therefore are wider than the observed ones, particularly at the most oblique angles (D cameras).

Changes in the symmetry of the distributions, as measured by their skewnesses, are illustrated in Fig. 6c. As with the means, the tendency of angular dependence is captured by the model, but the magnitude of change is underestimated, primarily because simulated clouds have sharper boundaries. Consequently, there are fewer and smaller areas of low reflectance in the simulated radiance field.

Although the mean, standard deviation, skewness and other low order moments provides some measure of variability, other statistical tools are needed to characterize the structure of the radiance fields. The power or energy spectrum, which represents a scale-by-scale decomposition of variance as captured by Fourier modes, is one of the tools that have been actively used in the analysis of the cloud observations (e.g., Cahalan & Snider, 1989; Davis et al., 1997; Sachs et al., 2002). The power spectrum is a convenient way to characterize scale invariant phenomena, for which the spectral density dependence on the wavenumber k

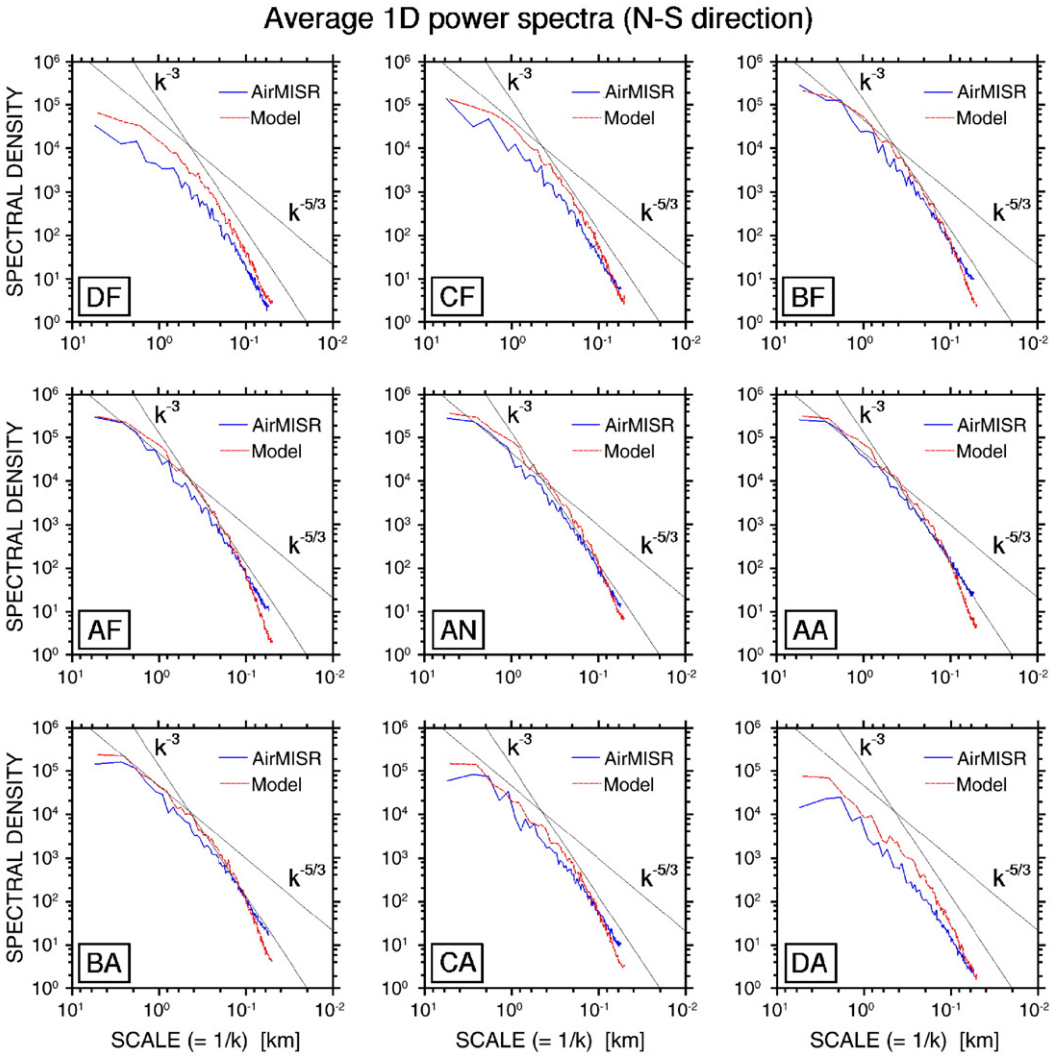

Fig. 7. 1D energy spectra of the radiance. The observed and simulated spectra are averaged over 200 vertical line scans from the fields shown in Figs. 3 and 4, respectively and, therefore, represent scale-by-scale decomposition of variance in the North–South direction. The scale break is seen at ~400 m. The −3 and −5/3 power-law dependencies of the wavenumber spectra are shown for reference.

takes the power-law form of k^s, where s is the scaling exponent. Fig. 7 show energy spectra of the simulated and observed radiance fields plotted against the horizontal scale ($1/k$) in log–log axes. Spectra are computed for each of the 200 vertical scan lines (columns) from respective images (Figs. 3 and 4) and averaged to reduce the noise. The represented scales for the model range from 5 km (5.5 km for observations), which is the size of the domain, to 50 m (55 m for observations), which is twice the pixel size.

For the nadir view (AN), the observed and simulated spectra show remarkable agreement. The slopes are similar and at smaller scales follow the k^{-3} wavenumber dependency, representative of a 3D isotropic turbulent flow. Cahalan and Snider (1989) using reflectances measured by the Band 2 (0.52–0.60 μm) of the Landsat's Thematic Mapper (TM) found similar scaling exponents: −3 for the fair weather cumulus and −3.6 for stratocumulus. The invariance at larger scales initially follows Kolmogorov's −5/3 slope and then flattens out at scales approaching the size of the domain. The scaling of both simulated and observed radiance fields breaks at about 400 m. Davis et al. (1997) linked of the radiative smoothing scale η to cloud properties through $\eta \approx H((1-g)\tau)^{-0.5}$, where H is cloud geometric thickness, g the asymmetry factor and τ the mean optical thickness. For the simulated case, representative values of $H=600$ m, $g=0.85$, and $\tau=25$, result in an estimate of $\eta \approx 310$ m, which is consistent with Fig. 7 considering that the transition between the two regimes is gradual.

If we plot the same spectra for the East–West instead of North–South direction, i.e., apply the Fourier analysis to horizontal (i.e., rows) rather than vertical (i.e., columns) scan lines on images in Figs. 3 and 4, we notice that for the near-nadir views the observed spectra do not change much but the simulated ones become steeper at small scales (Fig. 8).

4. Summary and discussion

Performance of a high-resolution cloud model is evaluated in a closure experiment which consists of using available observations to initialize and drive a model and then evaluating the model output using an independent set of measurements. In a case study of continental stratocumulus, a three-dimensional radiative transfer model is applied to synthetic cloud properties

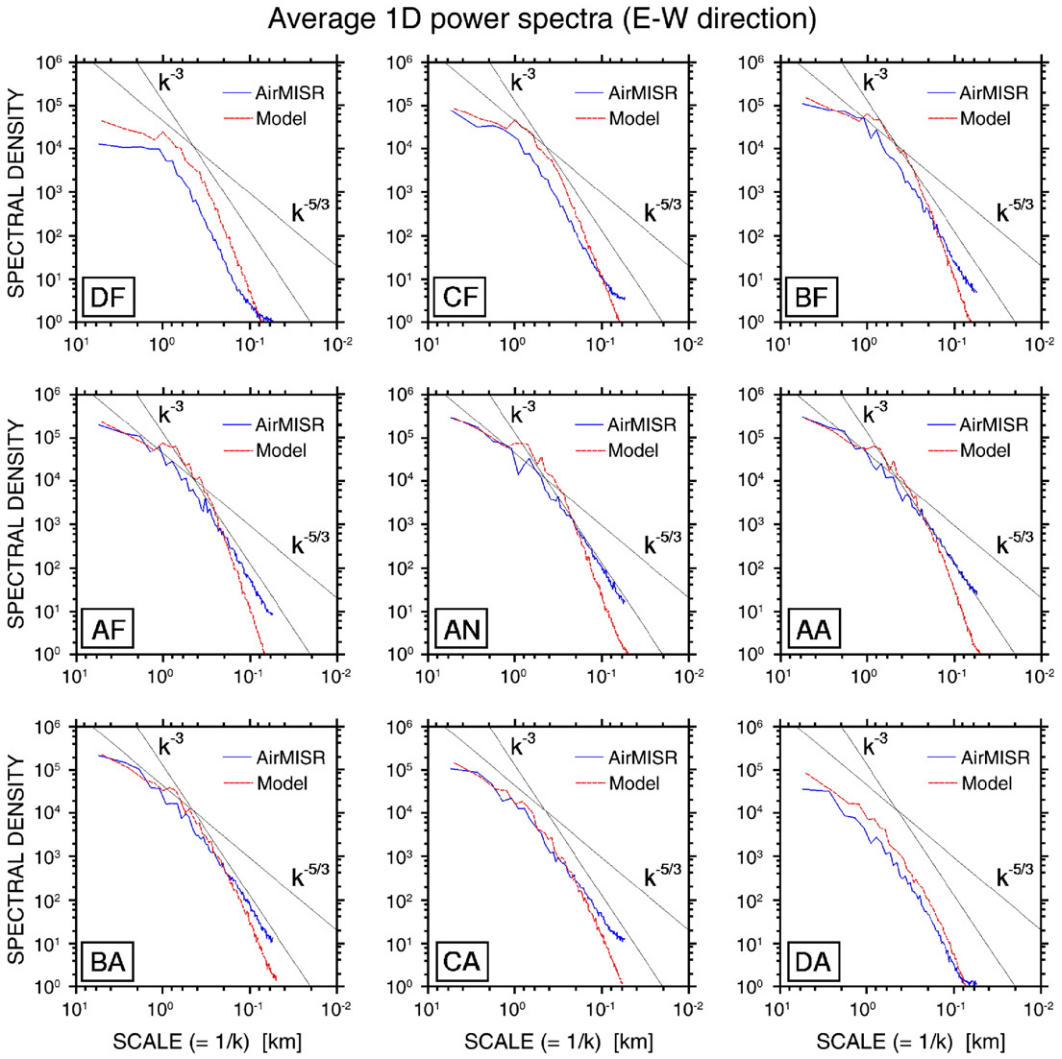

Fig. 8. Same as Fig. 7 but for spectra averaged over horizontal scan lines, thus representing scaling along the East–West direction.

generated by the cloud model in order to simulate top of the atmosphere radiances. The radiances computed for 0.443-μm wavelength are compared to observations from the blue channel of the airborne Multiangle Imaging Spectroradiometer (AirMISR) flown on NASA's ER-2 aircraft. By simulating and analyzing radiance distributions for all nine camera angles, we subject the modeled cloud structure to a much more stringent test than in previous studies.

Comparison of the domain averaged statistics demonstrates qualitative agreement and reveals several model biases (Fig. 6). Both simulated and observed fields show a minimum in the mean radiance at the near-nadir viewing angles but the model overestimates that minimum. Simulations match well the increased reflectance at more oblique angles. The model qualitatively captures the angular changes in the width and symmetry of radiance distribution, as measured by the standard deviation and skewness, but again underestimates the magnitude of this change for different viewing angles.

There are uncertainties in our radiative transfer calculations related to the effects of underlying surface and vertical aerosol distribution. However, given the large cloud fraction combined with the low surface albedo (0.04) at the considered wavelength of 0.443 μm as well as low aerosol optical depth of about 0.1 on the studied day, the uncertainties in these factors are not nearly large enough to explain the observed differences. Positive model bias in the domain mean radiance at nadir indicates that the model may contain more condensate than the real cloud layer. However, Marchand and Ackerman (2004) were able to reproduce radiance distributions for two sub-patches of the studied AirMISR image using the mean vertical liquid water paths (LWPs) of 80 and 158 g m^{-2}. Therefore, the simulated domain mean LWP of 106 g m^{-2} may be closer to the reality of the scene than the comparison with the MWR retrieval at the time of the overpath would suggest (Fig. 2). Model overestimation of the mean reflectance is more likely to be due to prediction of a too narrow distribution of the LWP. This will also be consistent with the difference in slopes from nadir towards the far aft views (Fig. 6a) suggesting that the simulated cloud top is too smooth. We note that although some biases remains, model radiance distributions improved markedly from our earlier simulations using 50 and 100 m horizontal grid size. A future study should determine if the LWP and cloud top height distributions continue to improve with refinement of the grid size below 25 m, and whether these improvements will lead to a better representation of angular dependence of radiance.

Another factor contributing to the model biases could be that the droplet effective radius near the cloud top exceeds the cloud mean value of 6.8 μm used in the radiation transfer calculation. Increasing the effective radius would decrease the mean reflectance, more so for smaller optical paths, i.e., for smaller zenith viewing angles, thus resulting in stronger angular dependence.

The scale-by-scale decomposition of variance is analyzed using power spectra. This analysis shows that at scales under about 200 m the simulated radiance fields are consistently smoother than observations, except at the most oblique view angle (D cameras). Although the break in scaling of the horizontal radiance field at about 400 m is reproduced correctly, the model spectra at smaller scales generally follow a steeper slope than observed −3. Furthermore, the scaling of the simulated radiance fields is notably different for north–south and east–west transects (or equivalently along and across the mean wind, or cloud rolls), the latter ones being less variable at small scales. Interestingly, in Cahalan and Snider (1989), the spectrum computed from several scans across stratocumulus rolls followed a −3.6 slope, while the spectrum from a fair weather cumulus scene (with no preferential cloud orientation) yielded a −3 slope. Sachs et al. (2002) noted the potential sensitivity of 1D spectrum to the effects of horizontal anisotropy, which our simulated radiance fields clearly exhibit (Fig. 4), but we are not aware of any study quantifying this relation in stratocumulus. Another possible reason behind the simulated anisotropy is in the potential directional dependence of numerical diffusion in the model forced with relatively strong wind along one axis.

Although the robustness of the comparisons, causes for the found biases, and the sensitivity of the simulated radiance distributions to the model's formulations, such as resolution and treatment of cloud microphysics, all remain to be determined, the fact that simulated radiance fields look, in many respects, remarkably similar to observations is encouraging. The model's ability to realistically reproduce elements of radiance field structure at scales down to 50 m using only large-scale (hundreds of kilometers) information about the environment confirms that such models can indeed be used in bridging the scale gaps among various observations. With respect to model validation, however, one must keep in mind that an agreement between the simulated and observed radiance fields is necessary but not sufficient for claiming the correct prediction of cloud property distributions at and below the radiative smoothing scale (typically few hundred meters for low-level clouds). Other ground-based and in situ measurements must be drawn into analysis to evaluate simulations at smaller scales.

High-resolution cloud model simulations and the three-dimensional radiative transfer modeling conducted in this study are computationally very demanding. As such, they are not suitable for long term or ensemble runs, including operational applications. We see the practical outcome of this and similar studies in creating comprehensive datasets in which diverse emulated measurements are tied together in a physically consistent manner using realistic model-generated meteorological fields. Since the retrieval algorithms can be run on the simulated observations, these datasets provide a testbed for consistent evaluation of assumptions on cloud properties and cloud structure employed in satellite retrievals. One can also use the simulations to study how the properties of the cloud field affect the satellite observations and thus demonstrate the satellite measurement sensitivity to any given cloud property. That is, any property of the model cloud field can be modified and the instrument-simulated data examined to determine if the change in this property significantly alters the statistics. We expect that this activity will expand rapidly as more and more of satellite-derived cloud products come from multi-sensor retrievals, for which obtaining a coherent description of the ground truth becomes increasingly difficult.

Acknowledgements

This study was supported by the National Space and Aeronautic Agency (NASA) through the Radiation Sciences Program. The AirMISR data were obtained from the NASA Langley Research Center Atmospheric Sciences Data Center. Other observations were obtained from the Atmospheric Radiation Measurement (ARM) Program data archive maintained by the Department of Energy. The Pacific Northwest National Laboratory is operated for the DOE by Battelle Memorial Institute under contract DE-AC06-76RLO 1830. Thoughtful comments by Howard Barker and two anonymous reviewers helped to improve the manuscript. We are grateful to Marat Khairoutdinov and Frank Evans for providing the CRM and SHDOM codes, respectively.

References

Barker, H. W., Goldstein, R. K., & Stevens, D. E. (2003). Monte Carlo simulation of solar reflectances for cloudy atmospheres. *Journal of the Atmospheric Sciences*, *60*, 1881−1894.

Barker, H. W, Pavloski, C. F., Ovtchinnikov, M., & Clothiaux, E. E. (2004). Assessing a cloud optical depth retrieval algorithm with model-generated data and the frozen turbulence assumption. *Journal of the Atmospheric Sciences*, *61*, 2951−2956.

Cahalan, R. F., & Snider, J. B. (1989). Marine stratocumulus structure. *Remote Sensing of Environment*, *28*, 95−107.

Chevallier, F., & Kelly, G. (2002). Model clouds as seen from space: Comparison with geostationary imagery in the 11-μm window channel. *Monthly Weather Review*, *130*, 712−722.

Davis, A., Marshak, A., Cahalan, R., & Wiscombe, W. (1997). The Landsat scale break in stratocumulus as a three-dimensional radiative transfer effect: Implications for cloud remote sensing. *Journal of the Atmospheric Sciences*, *54*, 241−260.

Diner, D. J., Beckert, J. C., Bothwell, G. W., & Rodriguez, J. I. (2002). Performance of the MISR instrument during its first 20 months in earth orbit. *IEEE Transactions on Geoscience and Remote Sensing*, *40*, 1449−1466.

Diner, D., Braswell, B., Davies, R., Gobron, N., Hu, J., Jin, Y., et al. (2005). The value of multiangle measurements for retrieving structurally and radiatively consistent properties of clouds, aerosols, and surfaces. *Remote Sensing of the Environment*, *97*, 495−518.

Evans, K. F. (1998). The spherical harmonics discrete ordinate method for three-dimensional atmospheric radiative transfer. *Journal of the Atmospheric Sciences*, *55*, 429−446.

Kato, S., Hinkelman, L. M., & Cheng, A. (2006). Estimate of satellite-derived cloud optical thickness and effective radius errors and their effect on computed domain-averaged irradiances. *Journal of Geophysical Research*, *111*, D17201. doi:10.1029/2005JD006668

Khairoutdinov, M. F., & Randall, D. A. (2003). Cloud resolving modeling of the ARM summer 1997 IOP: Model formulation, results, uncertainties, and sensitivities. *Journal of the Atmospheric Sciences*, *60*, 607−625.

Marchand, R., & Ackerman, T. P. (2004). Evaluation of radiometric measurements from the NASA multiangle imaging spectroradiometer (MISR): Two- and three-dimensional radiative transfer modeling of an inhomogeneous cloud deck. *Journal of Geophysical Research*, *109*, D18208. doi:10.1029/2004JD004710

Marchand, R., Ackerman, T. P., King, M. D., Moroney, C., Davies, R., Muller, J. -P. A. L., et al. (2001). Multiangle observations of Arctic clouds from FIRE ACE: June 3, 1998 case study. *Journal of Geophysical Research*, *106* (D14), 15,201−15,214. doi:10.1029/2000JD900302

Morcrette, J. -J. (1991). Evaluation of model-generated cloudiness: Satellite observed and model-generated diurnal variability and brightness temperature. *Monthly Weather Review*, *119*, 1205−1224.

Sachs, D., Lovejoy, S., & Schertzer, D. (2002). The multifractal scaling of cloud radiances from 1 m to 1 km. *Fractals*, *10*, 1−12.

Xie, S. C., Zhang, M., Branson, M., Cederwall, R. T., Del Genio, A. D., Eitzen, Z. A., et al. (2005). Simulations of midlatitude frontal clouds by single-column and cloud-resolving models during the Atmospheric Radiation Measurement March 2000 cloud intensive observational period. *Journal of Geophysical Research*, *110*, D15S03. doi:10.1029/2004JD005119

Zuidema, P., Davies, R., & Moroney, C. (2003). On the angular radiance closure of tropical cumulus congestus clouds observed by the multiangle imaging spectroradiometer. *Journal of Geophysical Research*, *108*(D20), 4626. doi:10.1029/2003JD003401